Journal of Fluids and Structures (1997) **11,** 693–716

CHAOS IN A HYDRAULIC CONTROL VALVE

S. HAYASHI,[1] T. HAYASE[1] AND T. KURAHASHI[2]

[1] *Institute of Fluid Science, Tohoku University, Sendai, Japan and*
[2] *Toyota Central Research Laboratory, Nagakute, Japan*

(Received 18 October 1995 and in revised form 7 February 1997)

In this paper we have studied the instability and chaos occurring in a pilot-type poppet valve circuit. The system consists of a poppet valve, an upstream plenum chamber, a supply pipeline and an orifice inserted between the pelnum and the pipeline. Although the poppet valve rests on the seat stably for a supply pressure lower than the cracking pressure, the circuit becomes unstable for an initial disturbance beyond a critical value and develops a self-excited vibration. In this unstable region, chaotic vibration appears at the period-doubling bifurcation. We have investigated the stability of the circuit and the chaotic phenomenon numerically, and elucidated it by power spectra, a bifurcation diagram and Lyapunov exponent calculations, showing that the phenomenon follows the Feigenbaum route to chaos.

1. INTRODUCTION

POPPET valves are pressure-regulating valves extensively used in hydraulic circuits. The circuits including the valve are classified into two categories: a direct-acting type and a pilot type. In the former the poppet valve is directly connected to a pipeline, while in the latter the valve is connected to a pipeline through an orifice and a plenum chamber. Both types of poppet valve circuits often become unstable, developing self-excited vibrations and often exhibiting irregular (chaotic) behaviour during self-excitation (Hayashi 1995).

The vibratory modes of the circuit consist of a poppet valve mode and an infinite number of pipeline modes corresponding to the natural frequencies of the fluid column in the connecting pipeline, infinite because of the continuous nature of the piepline. Thus, the dynamical behaviour of the system including the poppet valve is complex.

There have been many studies on the stability of the poppet valve circuit (Backé & Rünnenburger 1964; Funk 1964; Kasai 1968a,b). However, these studies have mainly treated local stability of the system, i.e., stability of the steady static points (fixed points). Little work has been done on global stability, self-excited vibrations and chaotic phenomena in this system.

One of the authors has indicated in a previous study that various kinds of chaotic vibrations occur in a direct-acting poppet valve circuit with a long lossless pipeline (Hayashi & Mochizuki 1987; 1989). In that study, it was found that the pipeline mode vibrations become unstable in turn starting from low frequency modes with increasing pipeline length. The system was found to have multiple unstable modes for a long pipeline. As a result, the system exhibits diverse self-excited vibrations, including period-doubling, almost periodic vibration composed of two unstable modes of vibration, phase-locking phenomena between two unstable modes, and chaotic vibration.

0889–9746/97/060693 + 24 $25.00/fl970096

Using numerical simulation and experiments, the possibility of Feigenbaum-type chaos was shown for a relatively short pipeline circuit and Lorenz-type chaos and intermittent-type chaos for a long pipeline circuit.

Similarly to the direct-acting poppet valve, chaotic vibration is expected to occur in a pilot-type poppet valve circuit. Hayashi & Ohi (1993) perfromed numerical analysis for the case with a short supply pipeline. It was found that, even when the valve stably rests on the valve seat for a supply pressure lower than the cracking pressure, self-excited vibration occurs if a disturbance larger than a critical value is given to the poppet valve. This means the system undergoes subcritical instability. Occurrence of the chaotic vibration, however, has still not been confirmed in this self-excited vibration regime.

In the present study, the authors perform detailed numerical analysis on the chaotic vibration occurring in a pilot-type poppet valve circuit with a short pipeline. The dynamics can be approximated by a lumped parameter model. The numerical analysis shows that the resulting self-excited vibration undergoes transition, changing from a period-one vibration to a chaotic vibration through a period-doubling bifurcation cascade, with the supply pressure as a system parameter.

2. GOVERNING EQUATIONS

Figure 1 is a schematic diagram of a pilot-type poppet valve circuit considered here. The valve function is to keep the circuit pressure constant in case of excess flow in hydraulic systems. The working fluid flows from a constant pressure supply tank, passes through a pipeline, an orifice and a valve chamber, and flows out to the atmosphere from the poppet valve when the supply pressure exceeds the 'cracking' pressure P_{Si}, which is pre-adjusted by the spring supporting the poppet valve.

Governing equations describing the behaviour of the system are derived referring to Figure 1. The equation of motion of the poppet is described as a vibratory system with a single degree of freedom; thus,

$$m\frac{\mathrm{d}^2X}{\mathrm{d}t^2}+\delta\frac{\mathrm{d}X}{\mathrm{d}t}+kX+f_0=F, \tag{1}$$

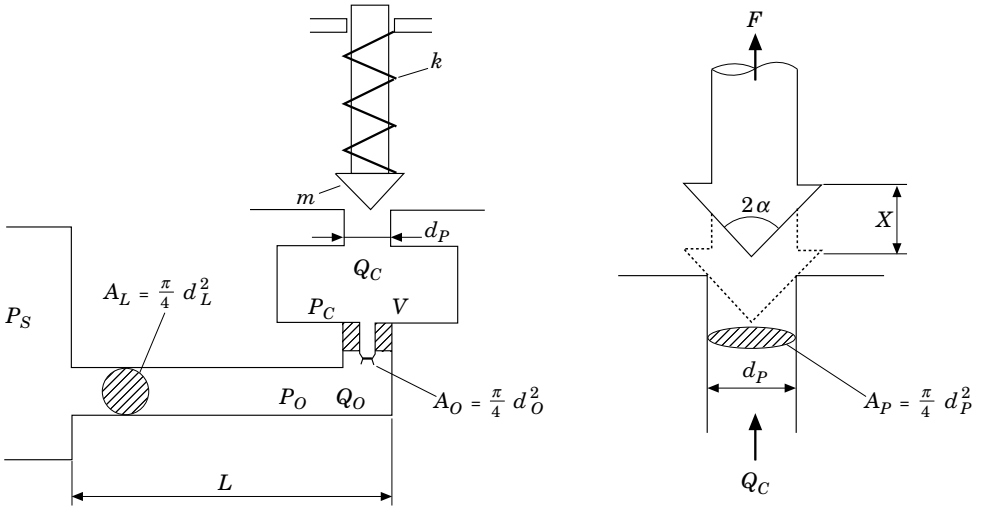

Figure 1. Schematic diagram of a poppet valve circuit of pilot type.

where X is the valve displacement (valve lift), m the mass of the poppet, δ the viscous damping coefficient, k the stiffness of the spring supporting the poppet, and f_0 the initial spring compression force. f_0 may be varied in order to pre-adjust the cracking pressure P_{Si} at which the valve begins to open, according to

$$f_0 = kX_i = A_P P_{Si}, \tag{2}$$

where X_i is the initial spring compression and A_P the cross-sectional area of the valve-seat aperture. F is the axial flow force acting on the poppet. For a sharp-edged valve seat, this axial force is given by (Takenaka & Urata 1975)

$$F = A_P P_C[1 - 4C_P(X/d_P)\sin 2\alpha], \tag{3}$$

where P_C is the valve chamber pressure, C_P the discharge coefficient of the poppet valve [see equation (7) below], d_P the diameter of the valve-seat aperture, and α the half-angle of the poppet.

The capacitive characteristic of the valve chamber is described by

$$\frac{V}{\beta}\frac{\mathrm{d}P_C}{\mathrm{d}t} = Q_O - Q_C, \tag{4}$$

where Q_O is the orifice flow rate, Q_C the poppet valve flow rate, V the valve chamber volume, and β the bulk modulus of the working fluid.

Since the supply line length is assumed to be short ($L = 0{\cdot}3$ m), the dynamics of the pipeline can be approximated by the lumped parameter model

$$\frac{\rho L}{A_L}\frac{\mathrm{d}Q_O}{\mathrm{d}t} = P_S - P_O, \tag{5}$$

where P_S is the supply pressure, L the length of the pipeline and A_L the cross-sectional area of the pipeline.

The flow rate through the poppet valve is

$$Q_C = C_P \pi d_P X \sin\alpha \sqrt{\frac{2\boldsymbol{\Psi}(P_C)}{\rho}}, \tag{6}$$

where d_p is the diameter of the valve seat, ρ is the density of the working fluid, and C_P is the discharge coefficient of the poppet valve, which changes almost linearly for small valve lift and becomes constant for large valve lift. Thus, it is approximated on the basis of the experimental results shown in Figure 2 by the following formula:

$$C_P = C_{PO}\left(\frac{\gamma X}{1 + \gamma X}\right), \tag{7}$$

where $C_{PO} = 0{\cdot}8$ and $\gamma = 40\,000\ \mathrm{m}^{-1}$. $\boldsymbol{\Psi}(P_c)$ is a function defined as follows:

$$\boldsymbol{\Psi}(P_C) = \begin{cases} P_C & \text{for } P_C > 0 \\ 0 & \text{for } P_C < 0. \end{cases} \tag{8}$$

When the pressure in the valve chamber drops below atmospheric pressure in the actual system, air dissolved in the working fluid is released and forms a cavity. As a result, the chamber pressure is maintained at atmospheric pressure. $\boldsymbol{\Psi}(P_C)$ in equation (6) simulates this actual situation.

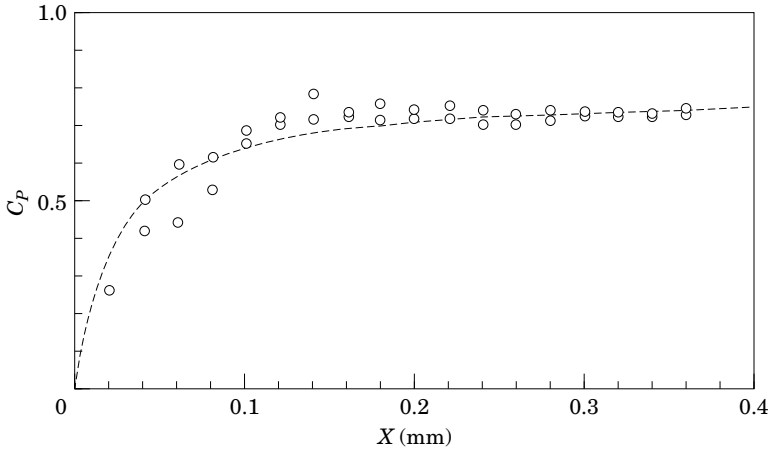

Figure 2. Experimental result for discharge coefficient of poppet valve ($d_P = 6$ mm, $P_{Si} = 4$ MPa): (– – –) $C_P = 0{\cdot}8\gamma X/(1 + \gamma X)$; (○), experimental.

The orifice flow Q_O is

$$Q_O = C_O A_O \operatorname{sgn}(P_O - P_C)\sqrt{\frac{2\,|P_O - P_C|}{\rho}}, \tag{9}$$

where C_O is the discharge coefficient of the orifice and A_O the area of the orifice.

The vibrating poppet sometimes impacts against the valve seat. In particular, this inevitably occurs for supply pressures below the crackling pressure. The following collision condition is applied in the numerical simulation

$$\dot{X}(t^+) = -e\dot{X}(t^-), \qquad X(t^\pm) = 0, \tag{10}$$

where $\dot{X}(t^-)$ and $\dot{X}(t^+)$ are the valve velocities just before and after collision, respectively, and e is the restitution coefficient.

To recapitulate, the set of governing equations may be summarized as follows:

$$\begin{aligned}
&m\ddot{X} + \delta\dot{X} + k(X + X_i) = A_p P_C\left[1 - 4C_{po}\left(\frac{\gamma X^2}{1 + \gamma X}\right)\frac{1}{d_P}\sin 2\alpha\right],\\
&\dot{P}_C = \left(\frac{\beta}{V}\right)\left[Q_O - C_{PO}\left(\frac{\gamma X^2}{1 + \gamma X}\right)\pi d_P \sin\alpha\sqrt{\frac{2\boldsymbol{\Psi}(P_C)}{\rho}}\right],\\
&\dot{Q}_O = \left(\frac{A_L}{\rho L}\right)\left[P_S - P_C - \frac{\rho}{2C_O^2 A_O^2}\,|Q_O|\,Q_O\right],\\
&\dot{X}(t^+) = -e\dot{X}(t^-), \qquad X(t^\pm) = 0.
\end{aligned} \tag{11}$$

The nonlinear simultaneous equations (11) for the unknown variables X, P_C and Q_O are numerically solved by the Runge–Kutta (R–K) method. The calculation is mainly carried out for a supply pressure lower than the cracking pressure of the valve; thus, the poppet inevitably collides against the valve seat, as stated previously. In general, the collision occurs in the interval of meshpoints of time in the numerical calculation. The total accuracy of the numerical solution is markedly reduced, if the collision time instant is calculated by the ordinary, simple linear interpolation; if $X(t_n)X(t_{n+1}) < 0$, then the instant of collision is given as $[X(t_{n+1})t_n - X(t_n)t_{n+1}]/[X(t_{n+1}) - X(t_n)]$. The calculation here is performed by using the "time stepsize subdivision method"

TABLE 1
System parameters used in simulation

Quantity	Symbol	Value	Units
Discharge coefficient of oriffice	C_O	0·64	
Valve diameter	d_P	$6{\cdot}0\times10^{-3}$	m
Orifice diameter	d_O	$2{\cdot}0\times10^{-3}$	m
Pipeline diameter	d_L	$8{\cdot}9\times10^{-3}$	m
Restitution coefficient	e	0·65	
Spring stiffness	k	$1{\cdot}284\times10^{4}$	N/m
Pipeline length	L	0·3	m
Valve mass	m	$7{\cdot}4\times10^{-2}$	kg
Valve chamber volume	V	$8{\cdot}1\times10^{-6}$	m^3
Half angle of poppet	α	45	deg
Bulk modulus	β	$1{\cdot}484\times10^{9}$	N/m^2
Damping coefficient	δ	4·905	kg/s
Density of fluid	ρ	$8{\cdot}563\times10^{2}$	kg/m^3

proposed by one of the authors (Hayashi, Iizuka & Hayase 1994a), which makes the accuracy of calculation for the collision instant to match that of the R–K method, by iteratively reducing the time step-size between two nodal points of time t_n and t_{n+1} containing a collision point.

The system parameters used in the simulation are listed in Table 1.

To perform the computations, the Cray Y-MP/8 in the Institute of Fluid Science, Tohoku University was used. This computer has 16 significant digits in decimal numeration for single precision arithmetic. The time step-size used was $h = 1{\cdot}0\times10^{-7}$ s. The highest frequency of the self-excited vibration considered here is about $f_n \simeq 1050$ Hz, as seen from the power spectra to be shown later, so the dimensionless time step-size is $H = f_n h = 1{\cdot}05\times10^{-4}$. Considering that a rough indication of the accumulated error of the R–K method is of the order of h^4, the total accuracy of the calculation is satisfactory.

3. LOCAL STABILITY

As a starting point for the analysis, a study of the local system stability is performed. To facilitate this, equations (11) are linearized at a static state ($X_{\mathrm{E}}, P_{C\mathrm{E}}$ and $Q_{O\mathrm{E}}$) to the following form:

$$
\begin{aligned}
&m\ddot{x} + \delta\dot{x} + kx = a_P p_c - k_X x,\\
&\dot{p}_C = \left(\frac{1}{C}\right)(q_O - c_P p_C - c_X x),\\
&\dot{q}_O = -\left(\frac{1}{I}\right)\left(p_C + \frac{1}{c_O}\, q_O\right),\\
&C = \frac{V}{\beta}, \qquad I = \frac{\rho L}{A_L}, \qquad a_P = \left(\frac{\partial F}{\partial P_C}\right)_{\mathrm{E}}, \qquad k_X = -\left(\frac{\partial F}{\partial X}\right)_{\mathrm{E}},\\
&c_P = \left(\frac{\partial Q_C}{\partial P_C}\right)_{\mathrm{E}}, \qquad c_X = \left(\frac{\partial Q_C}{\partial X}\right)_{\mathrm{E}}, \qquad c_O = \frac{C_O^2 A_O^2}{\rho Q_{O\mathrm{E}}},
\end{aligned}
\tag{12}
$$

where the variables x, p_C and q_O represent variational quantities from static state

values A_E, P_{CE} and Q_{OE}, in which the subscript E indicates the values at the steady static state, which are obtained for the given P_{Si} ($=kX_i/A_P$) and P_S from the following equations:

$$k(X+X_i) = A_P P_C\left[1 - 4C_{P0}\left(\frac{\gamma X^2}{1+\gamma X}\right)\frac{1}{d_P}\sin 2\alpha\right],$$

$$Q_O - C_{PO}\left(\frac{\gamma X^2}{1+\gamma X}\right)\pi d_P \sin\alpha\sqrt{\frac{2P_C}{\rho}} = 0, \tag{13}$$

$$P_S - P_C - \frac{\rho}{2C_O^2 A_O^2}Q_O^2 = 0.$$

The characteristic equation is derived from equation (12), i.e.,

$$s^4 + A_3 s^3 + A_2 s^2 + A_1 s + A_0 = 0, \tag{14}$$

where

$$\omega_P^2 = \frac{k+k_X}{m}, \qquad \omega_L^2 = \frac{1+c_P/c_O}{CI},$$

$$2\zeta_P\omega_P = \frac{\delta}{m}, \qquad 2\zeta_L\omega_L = \frac{c_P}{C} + \frac{1}{CI},$$

$$A_0 = \omega_P^2\omega_L^2 + \left(\frac{a_P}{m}\right)\omega_L^2\frac{c_X}{c_O+c_P}, \tag{15}$$

$$A_1 = 2\zeta_P\omega_P\omega_L^2 + 2\zeta_L\omega_L\omega_p^2 + \frac{a_P c_X}{mC},$$

$$A_2 = \omega_P^2 + \omega_L^2 + (2\zeta_P\omega_P)(2\zeta_L\omega_L),$$

$$A_3 = 2\zeta_P\omega_P + 2\zeta_L\omega_L.$$

The stability condition is given as

$$A_1A_2A_3 - A_1^2 - A_0A_3 > 0. \tag{16}$$

Since this system has a small damping coefficient and a small pipeline resistance, all characteristic roots are obtained as complex conjugate pairs. Therefore, the unstable modes are always dynamically unstable.

Figure 3(a) shows the stability map of the poppet valve circuit calculated from equation (16) for the static valve lift X_E and the supply pressure P_S. It is noted that the static valve lift X_E is determined from equation (13) by specifying the supply pressure P_S and the cracking pressure P_{Si}. The solid line shows the critical curve below which the system is unstable. A dashed line shows the static characteristic of the valve lift X with the supply pressure P_S corresponding to the cracking pressure $P_{Si} = 4{\cdot}0$ MPa. The static valve lift moves along the abscissa for the supply pressure smaller than P_{Si}. However, it moves along the dashed curve when the supply pressure becomes larger than P_{Si}. The static state becomes unstable on the segments AB and CD of the curve. Figure 3(b) indicates a partially enlarged stability map for the small lift region of Figure 3(a) (the ordinate is scaled to $\sqrt{X_E}$). According to Figure 3(b), the valve is stable in the small lift region, including $X = 0$.

Figure 4 indicates the change of the natural frequencies (dotted lines) corresponding to the imaginary part of characteristic roots of the linearized system and the frequencies of self-excited vibrations obtained from the simulation (symbols ○ and

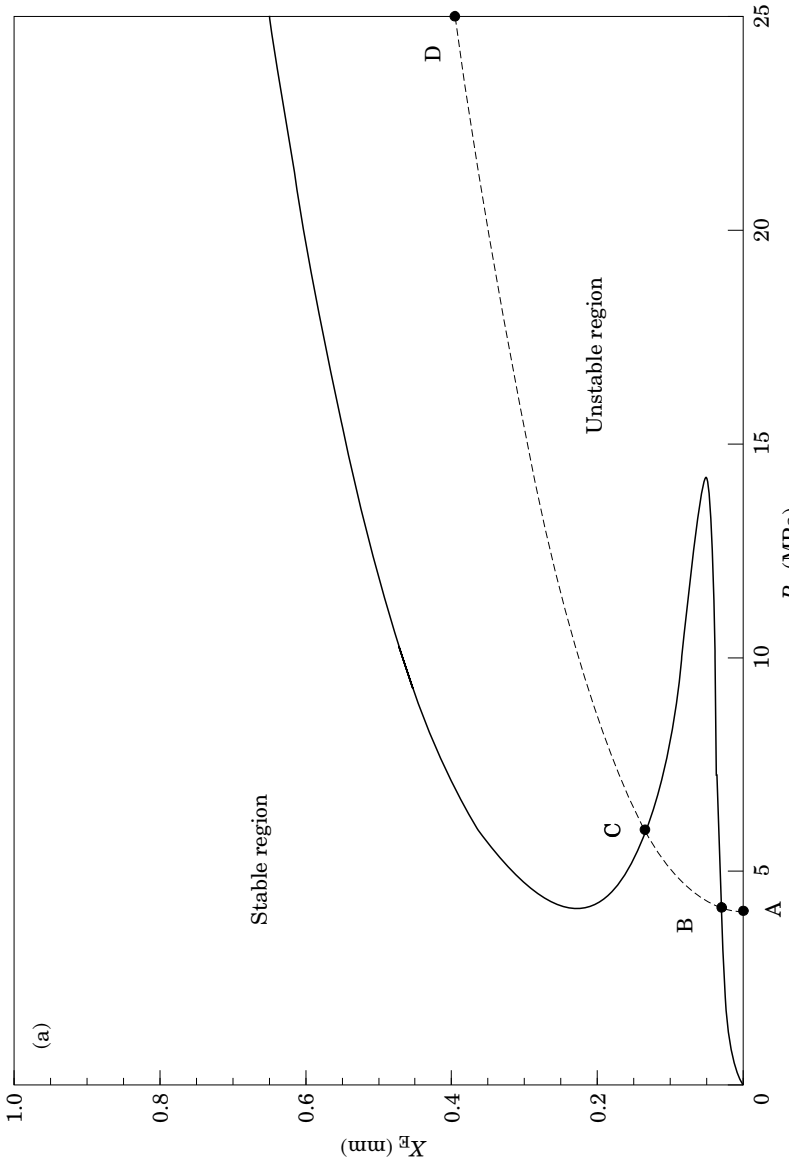

Figure 3. Stability map and steady valve lift with supply pressure: (a) Stability map over a wide area; (b) partly enlarged stability map; (– – –) $P_{Si} = 4{\cdot}0$ MPa.

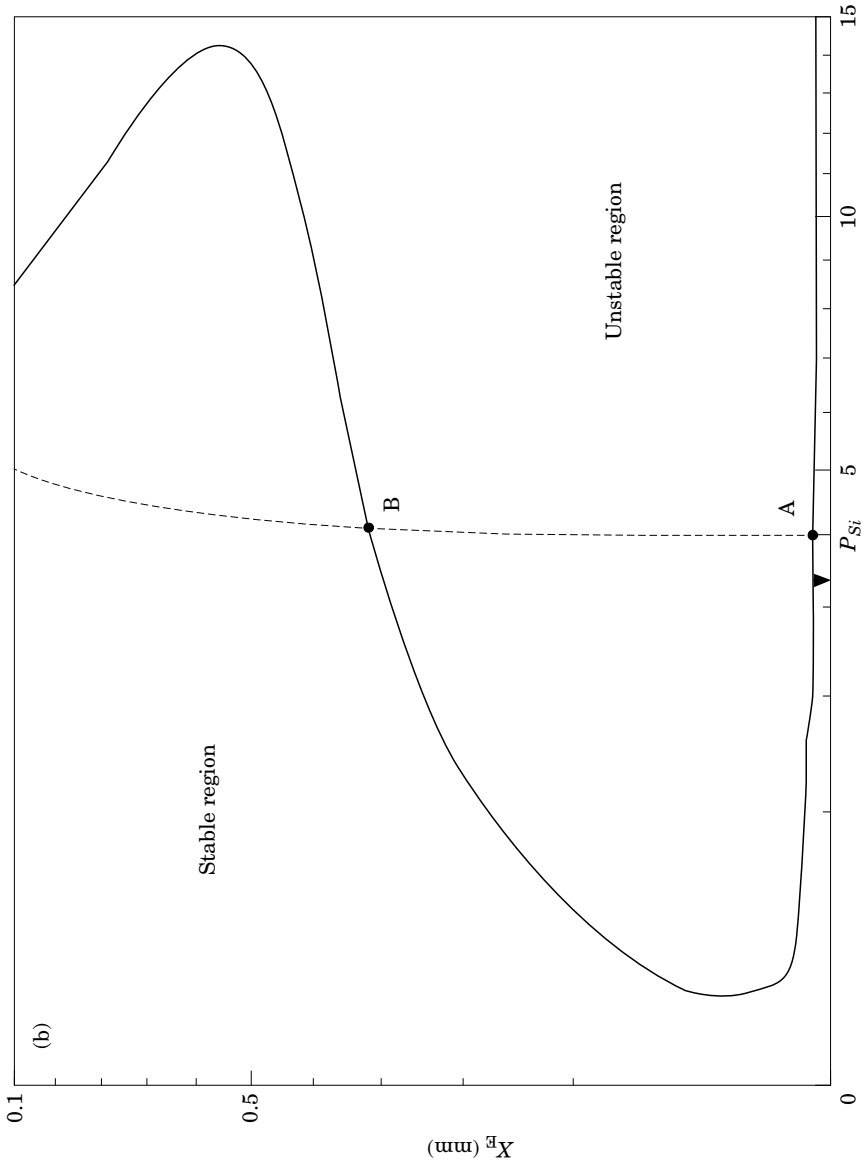

Figure 3. (*Continued.*)

●, respectively) with the supply pressure P_S. The natural frequencies of the linearized system at $P_S = P_{Si}$ (cracking pressure) coincide with those of the poppet valve and the pipeline-chamber system,

$$f_p = \frac{1}{2\pi}\sqrt{\frac{k}{m}}, \qquad \text{and} \qquad f_L = \frac{1}{2\pi}\sqrt{\frac{\beta A_L}{\rho V L}}, \tag{17}$$

respectively. Thus, we label the corresponding vibratory modes as the 'valve mode' and the 'pipeline mode', respectively. As seen from Figure 4, the pipeline mode is unstable on the segment AB and the valve mode on the segment CD (Hayashi, Hayase & Kurahashi 1994b).

Figure 4 shows that the self-excitation of the pipeline mode occurs even for a supply pressure lower than the cracking pressure P_{Si}. This implies that it is possible for self-excited vibration to occur due to large disturbances beyond a critical value, although the poppet in steady state rests on the valve seat stably, as seen in Figure 3(b); in other words, the instability is subcritical.

The situation is demonstrated in Figure 5, which shows the responses for slightly different initial velocities, for the system having an identical operating condition which is indicated by the symbol (▼) in Figure 3(b). For the smaller initial velocity in Figure 5(a), the poppet settles down to the original steady static state and rests on the seat again, while self-excited vibration develops as shown in Figure 5(b) for a slightly larger initial velocity. This is typical of hard self-excited vibration, i.e. of subcritical instability (Hayashi & Ohi 1988, 1993). This is conjectured to be caused by a shift of the equivalent static state into the unstable region shown in Figure 3(b); the centre of the poppet positional vibration in the pipeline mode is located at some distance from the valve seat due to the collision of the poppet against the seat. Chaotic phenomena occur in this region, accompanying the hard self-excited vibration.

4. CHAOTIC VIBRATION

A steady static point on the segment AB in Figure 3 is unstable, and a self-excited vibration in the piepline mode is excited from infinitesimal disturbances. This type of vibration is so-called "soft self-excited vibration". Once the vibration is self-excited, the vibration does not cease by lowering the supply pressure to below the cracking pressure, and the nature of the vibration shifts from soft self-excitation to the hard one. The vibration is maintained up to the considerably lower supply pressure of $P_S = 2{\cdot}8$ MPa, as seen in Figure 4.

4.1. Vibratory Waveforms, Power Spectra and Phase Plane Path

A change of vibratory waveform was examined numerically under the condition that the supply pressure was increased quasi-steadily from 3·0 MPa to 4·0 MPa. In the simulation, each calculation for a given supply pressure was performed until $t = 0{\cdot}25$ s in order to allow the system to attain a steady state vibration. The supply pressure P_S, which is the system parameter varied, was then slightly increased and, for the next step of the calculation, the last set of state variables were used as initial conditions.

The results are shown in Figure 6(a)–6(f). In each case, the uppermost figure shows the displacement X of the poppet, the centre figure the power spectrum of X/X_{ref} (the reference quantity $X_{\text{ref}} = 1$ m) and the bottom figure the phase-plane plot of X vs. $\dot{X}$.

In Figure 6(a) for $P_S = 3{\cdot}4$ MPa, the waveform of the vibration is almost sinusoidal with a frequency corresponding to the pipeline mode frequency. In Figure 6(b), for

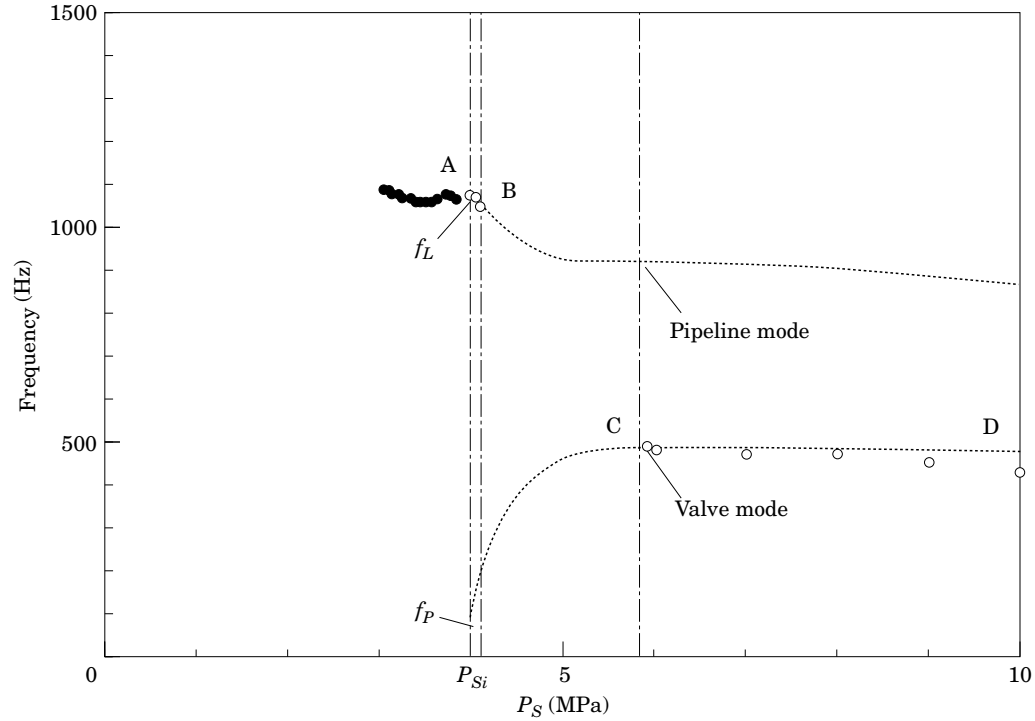

Figure 4. Natural frequencies of the system ($P_{Si} = 4{\cdot}0$ MPa): (●), hard self-excitation; (○), soft self-excitation.

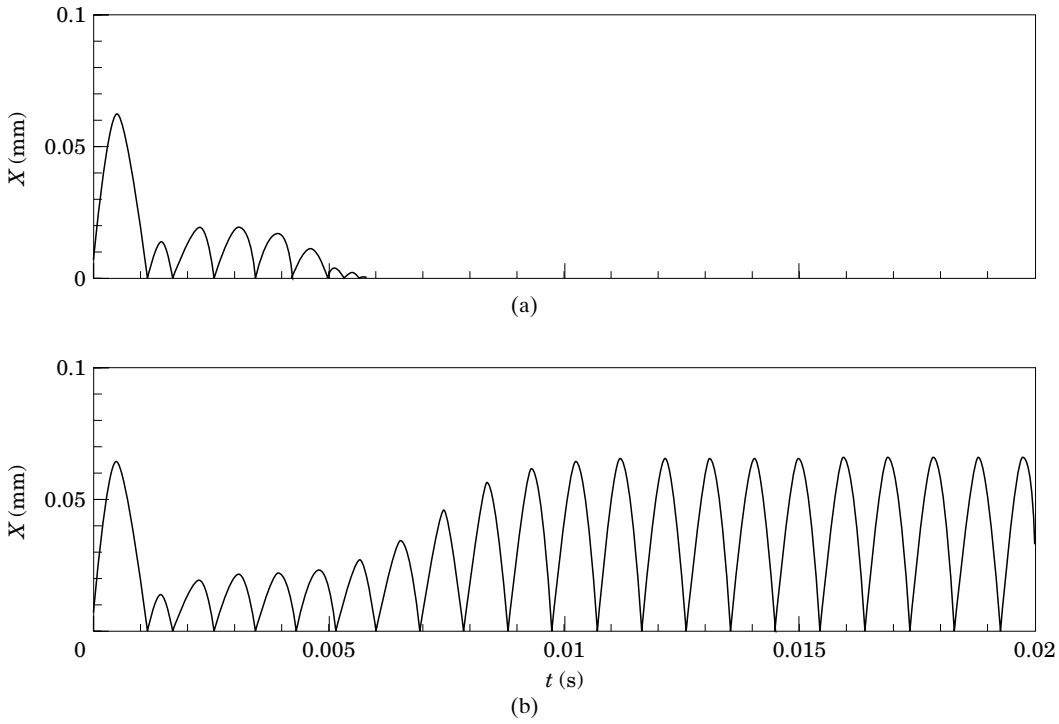

Figure 5. Responses of poppet valve for slightly different initial conditions: (a) initial velocity $\dot{X}(0) = 0{\cdot}212$ m/s, supply pressure $P_S = 3{\cdot}4$ MPa; (b) $\dot{X}(0) = 0{\cdot}215$ m/s, $P_S = 3{\cdot}4$ MPa.

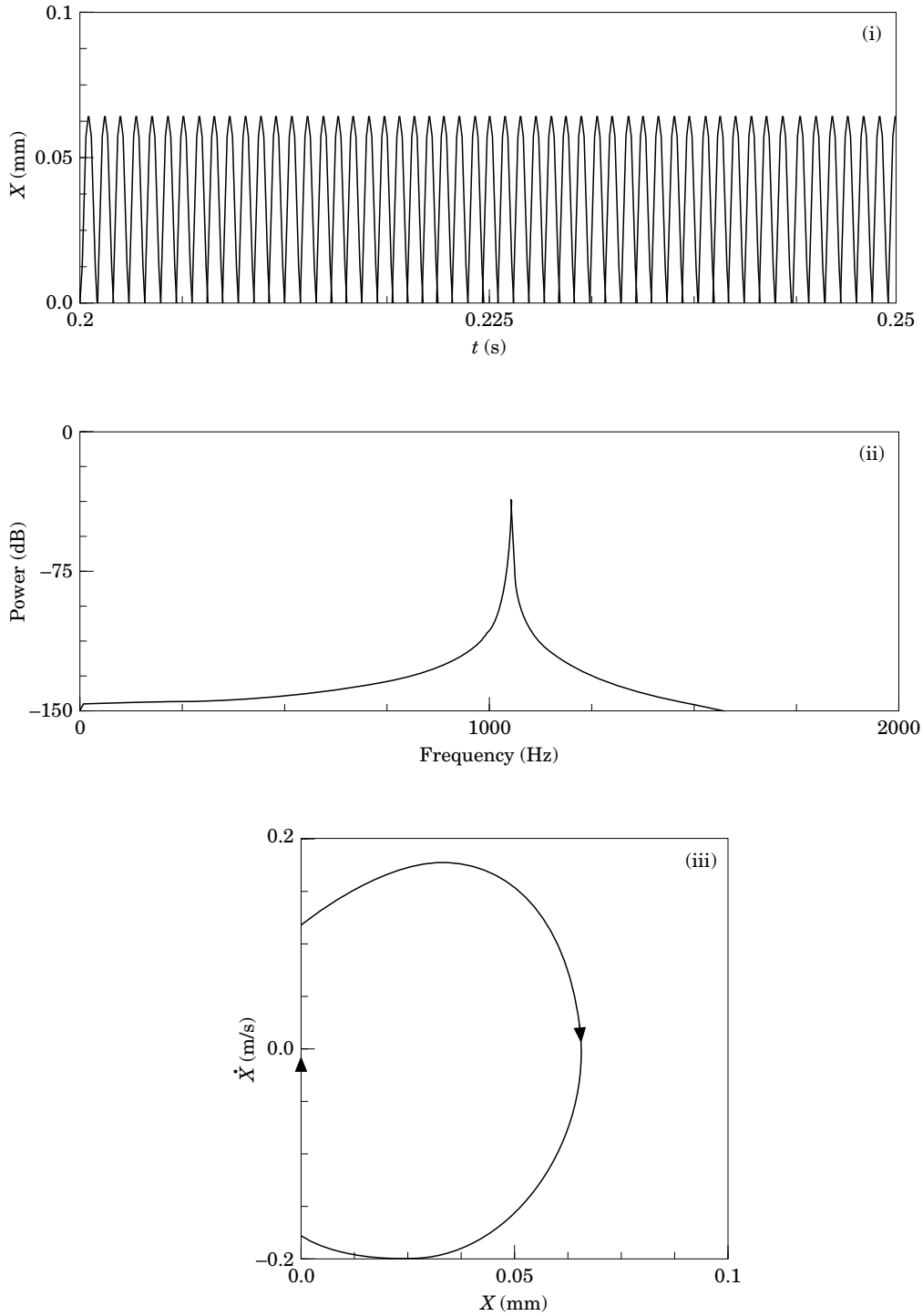

Figure 6(a). Comparison of self-excited vibrations in different supply pressure for $P_S = 3{\cdot}4$ MPa; period-one vibration: (i) poppet vibration; (ii) power spectrum; (iii) phase-plane plot.

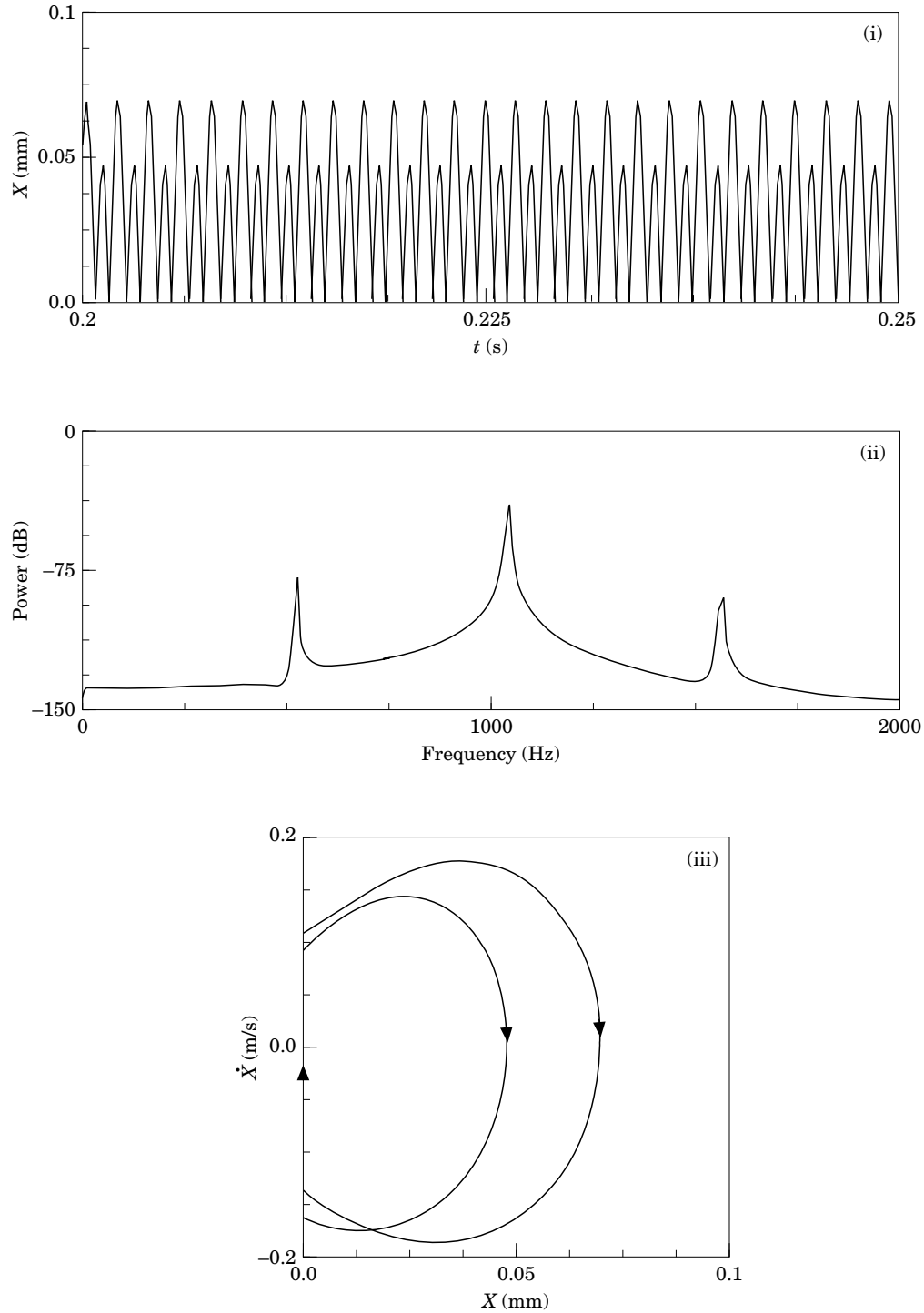

Figure 6(b). Comparison of self-excited vibrations in different supply pressure for $P_S = 3{\cdot}5$ MPa; period-two vibration. See key in Figure 6(a).

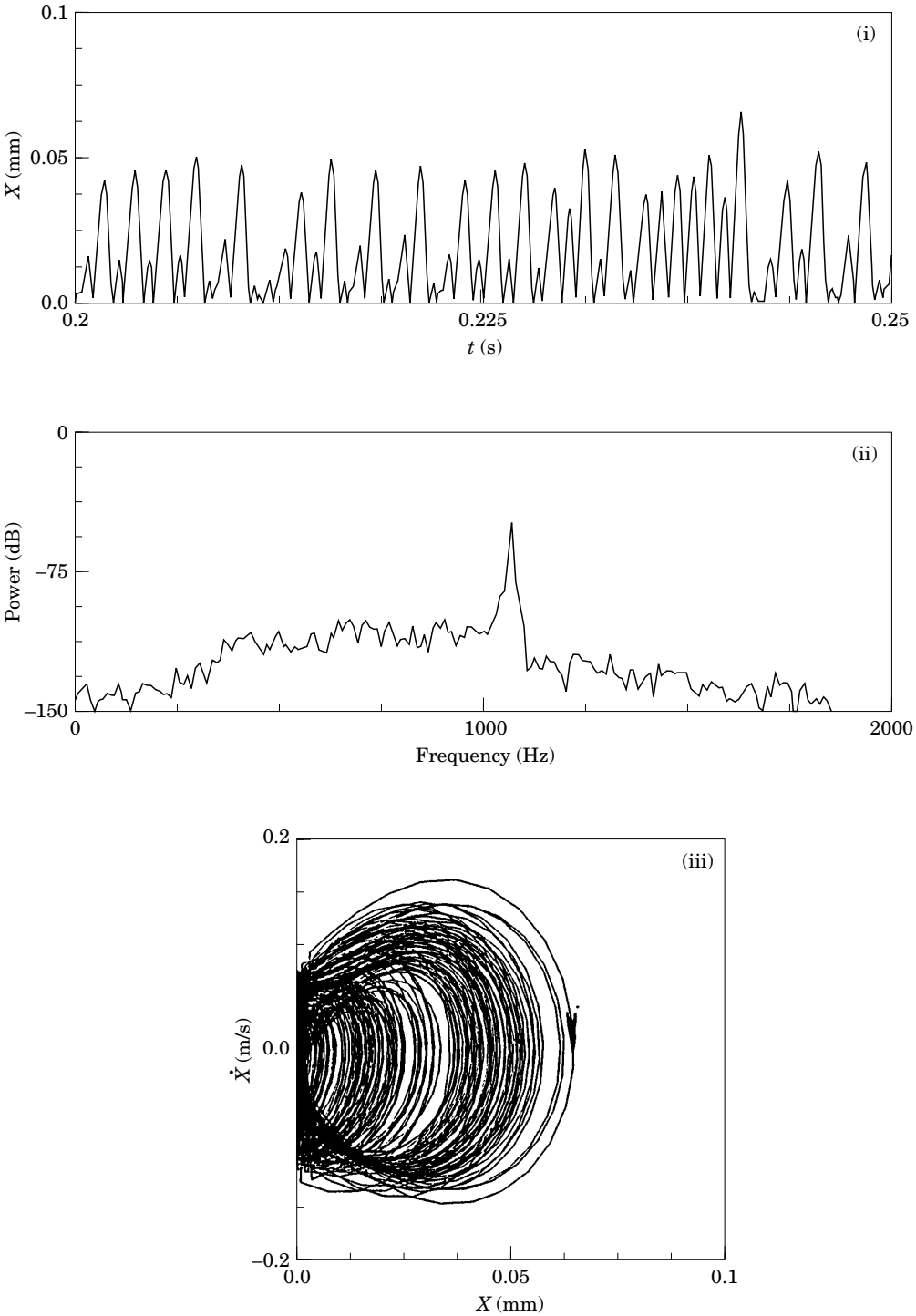

Figure 6(c). Comparison of self-excited vibrations in different supply pressure for $P_S = 3{\cdot}7$ MPa; chaotic vibration. See key in Figure 6(a).

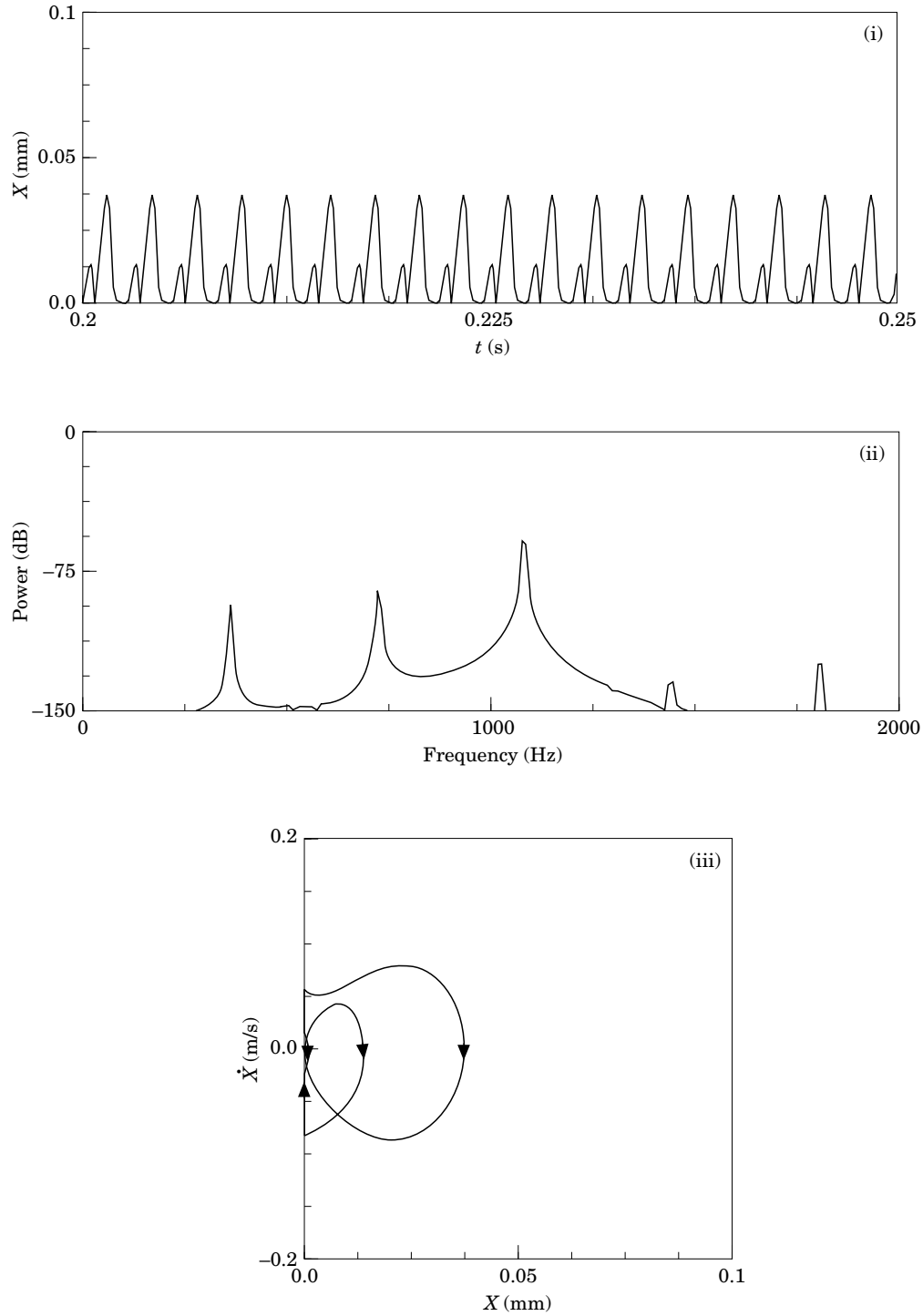

Figure 6(d). Comparison of self-excited vibrations in different supply pressure for $P_S = 3{\cdot}76$ MPa; period-three vibration. See key in Figure 6(a).

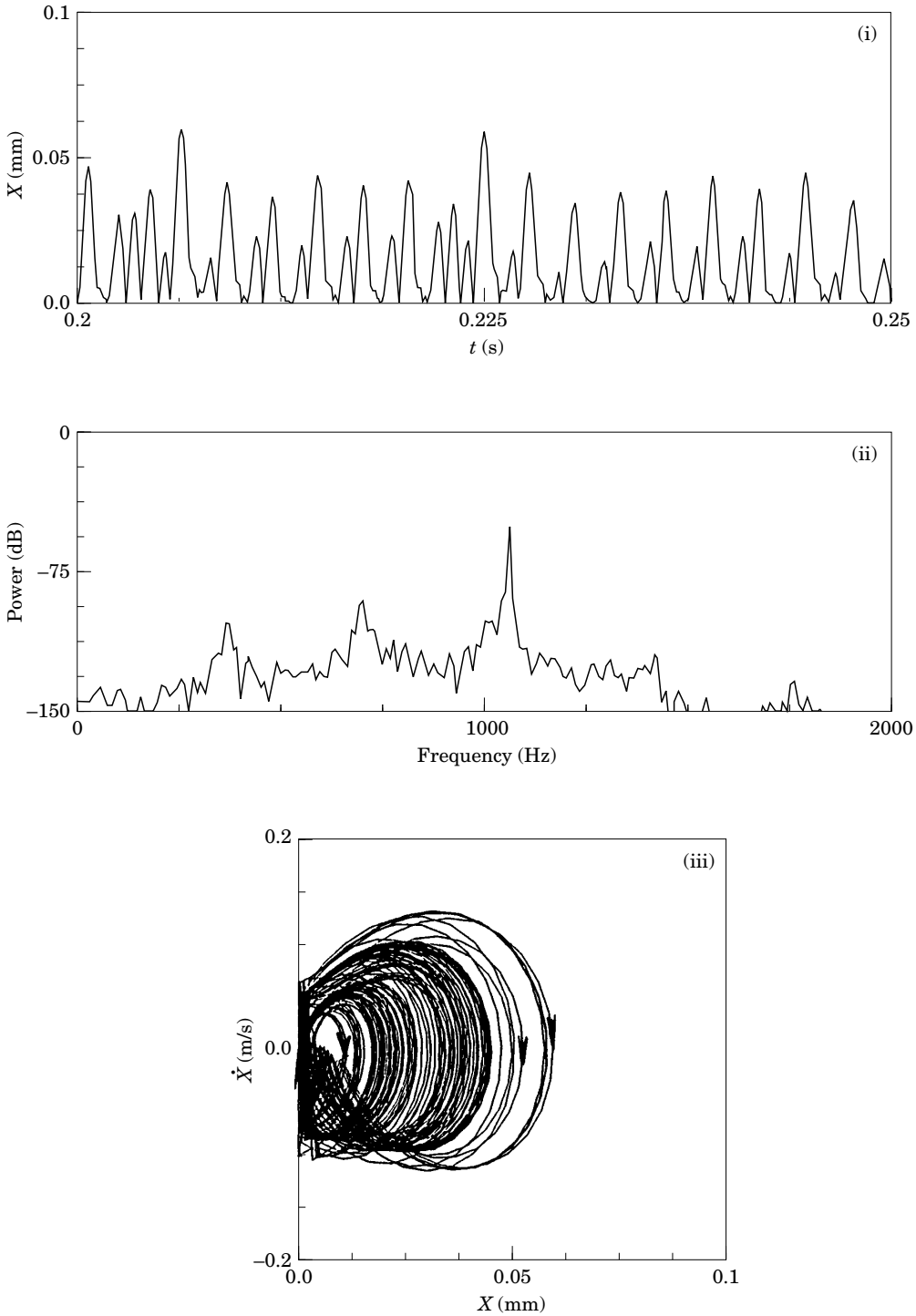

Figure 6(e). Comparison of self-excited vibrations in different supply pressure for $P_S = 3{\cdot}8$ MPa; chaotic vibration. See key in Figure 6(a).

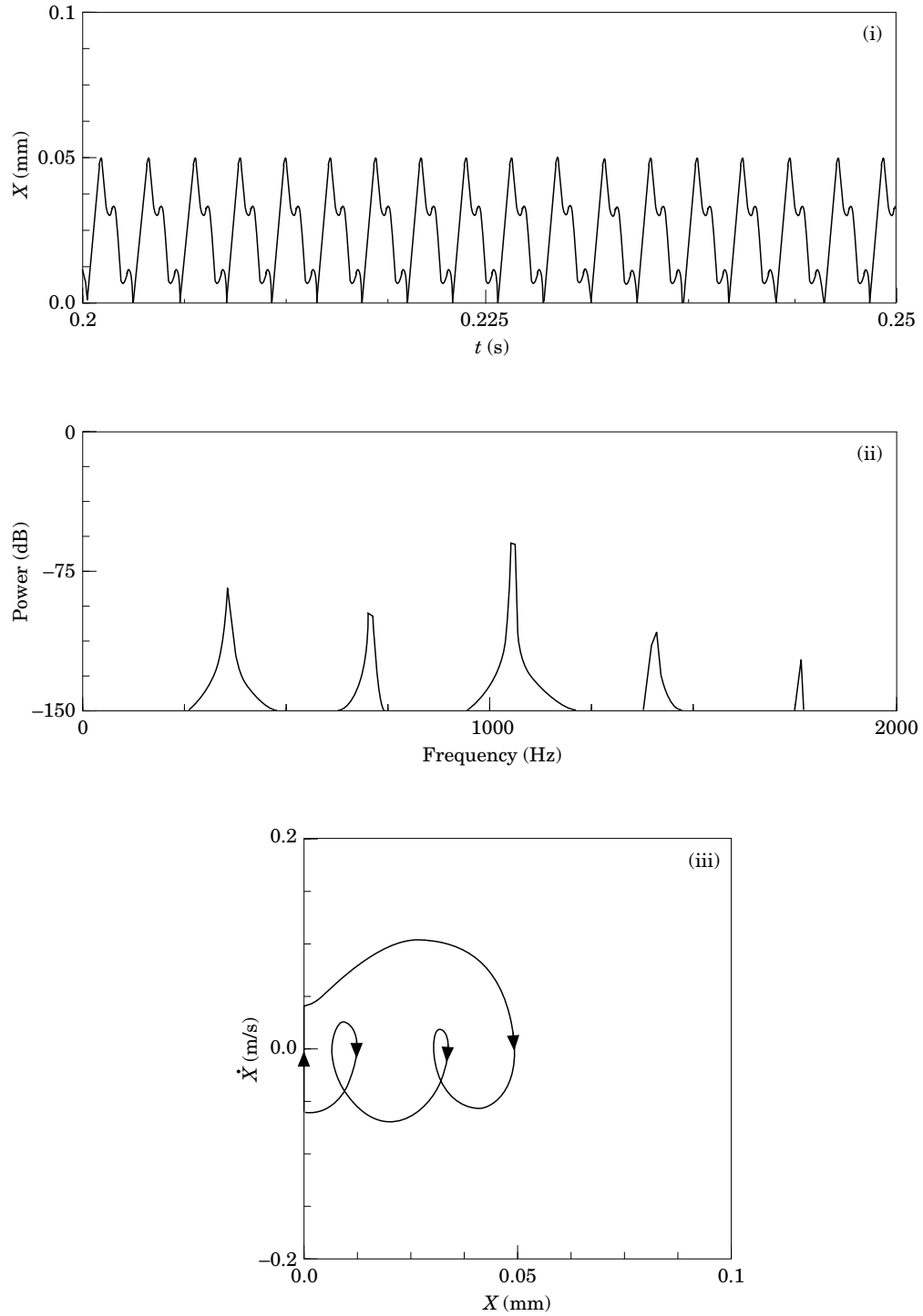

Figure 6(f). Comparison of self-excited vibrations in different supply pressure for $P_S = 4{\cdot}0$ MPa; period-three vibration. See key in Figure 6(a).

$P_S = 3{\cdot}5$ MPa, the response bifurcates to period-2 vibration. In Figure 6(c), for $P_S = 3{\cdot}7$ MPa, the vibration is chaotic. The power spectrum rises at all frequencies, while the peak width broadens. These are typical features of chaotic phenomena. Increasing P_S still further, the vibration changes to period-3 and then becomes chaotic once again, as shown in Figure 6(d) for $P_S = 3{\cdot}76$ MPa and (e) for $P_S = 3{\cdot}8$ MPa. For higher P_S, the vibration passes through period-2 and period-3 [Figure 6(f)] vibrations and finally it returns to period-1, which is a conventional self-excited vibration.

4.2. Bifurcation Diagram

Figure 7 is a bifurcation diagram on which all the maxima of the vibratory waves of the poppet displacement are plotted against supply pressure P_S. In this figure, the right-hand side dashed curve represents the static valve lift. The points A and B correspond to those in Figure 3; they indicate the stability boundary points. Other static points except the interval AB in the figure are locally stable as described previously.

The self-excited vibration undergoes a series of period-doubling bifurcations with increasing P_S leading to the first chaotic region. Figure 6(c) corresponds to the chaotic vibration occurring in this region. With further increase in P_S, a period-3 window corresponding to Figure 6(d) appears. At higher P_S still, the vibration enters the second chaotic regime. Figure 6(e) corresponds to the chaotic vibration occurring in this regime. The chaotic vibration disappears around $P_S = 3{\cdot}85$ MPa. The vibration goes through period-2 and period-3 and returns to period-1 vibration around the cracking pressure $P_S = 4{\cdot}0$ MPa.

The first period-doubling bifurcation sequence in Figure 7 is shown in detail in Figures 8(a), (b) and (c); Figures 8(b) and (c) are magnifications of the regions enclosed by squares in Figures 8(a) and (b), respectively. Bifurcation points obtained from the figures are listed in Table 2, where μ_n represents the bifurcation point from the period-2^{n-1} vibration to the period-2^n vibration. Table 2 shows that the ratio $\Delta_n = (\mu_{n-1} - \mu_{n-2})/(\mu_n - \mu_{n-1})$ approaches the Feigenbaum number $\Delta = \lim_{n\to\infty} \Delta_n = 4{\cdot}6692016\ldots$ (Feigenbaum 1980). The bifurcation sequence resembles very much the Feigenbaum route to chaos.

Assuming that the ratio Δ_n after $n = 6$ can be approximated by the Feigenbaum number, the point of accumulation $P_{S\mathrm{ac}}$ is estimated from Table 2 as

$$\begin{aligned} P_{S\mathrm{ac}} &= \mu_4 + (\mu_5 - \mu_4) + (\mu_6 - \mu_5) + (\mu_7 - \mu_6) + \ldots \\ &= \mu_4 + (\mu_5 - \mu_4) + (\mu_5 - \mu_4)\frac{1}{\Delta_6} + (\mu_5 - \mu_4)\frac{1}{\Delta_6\Delta_7} + \ldots \\ &\simeq \mu_4 + (\mu_5 - \mu_4) + (\mu_5 - \mu_4)\frac{1}{\Delta} + (\mu_5 - \mu_4)\frac{1}{\Delta^2} + \ldots \\ &\simeq \mu_4 + (\mu_5 - \mu_4)\frac{1}{1 - \dfrac{1}{\Delta}} \simeq 3{\cdot}634852, \end{aligned} \tag{18}$$

where $\mu_4 = 3.63409$, $\mu_5 - \mu_4 = 0{\cdot}000599$ and $\Delta = 4{\cdot}66920\ldots$. The accumulation point is indicated in Figure 8.

4.3. Lyapunov Exponents

Here we discuss the change of the largest Lyapunov exponent λ with supply pressure P_S used as the system parameter varied, by utilizing the method of Wolf *et al.* (1985) which makes use of time-series data of chaotic vibrations. The exponent λ is calculated as follows.

The state variables are defined as

$$Y = (X, \dot{X}, P_C, Q_O)^{\mathrm{T}}, \tag{19}$$

and the governing equations are expressed as

$$\dot{Y} = F(Y). \tag{20}$$

A solution of equation (20) for an appropriate initial condition Y_0 is taken as a fiducial

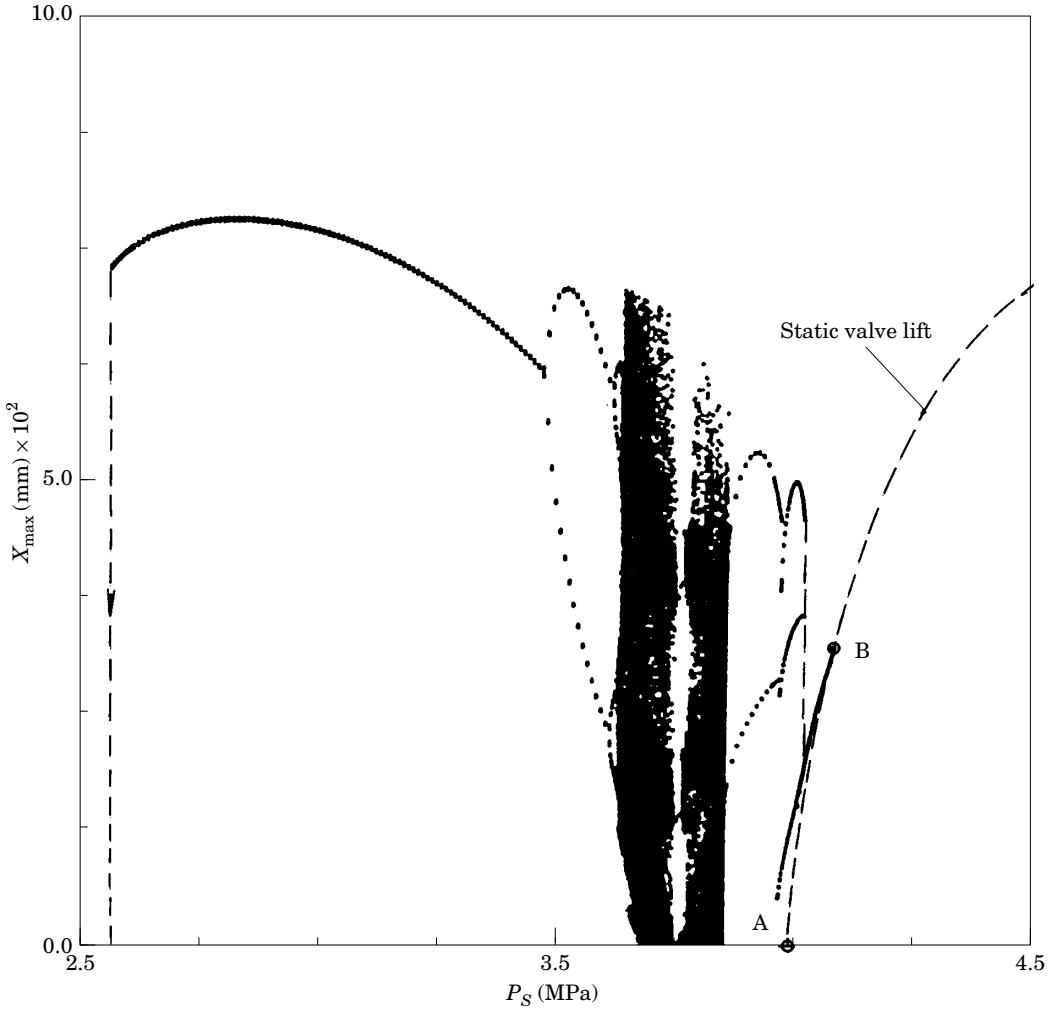

Figure 7. Bifurcation diagram of vibrations for operating point of $P_{Si} = 4{\cdot}0$ MPa.

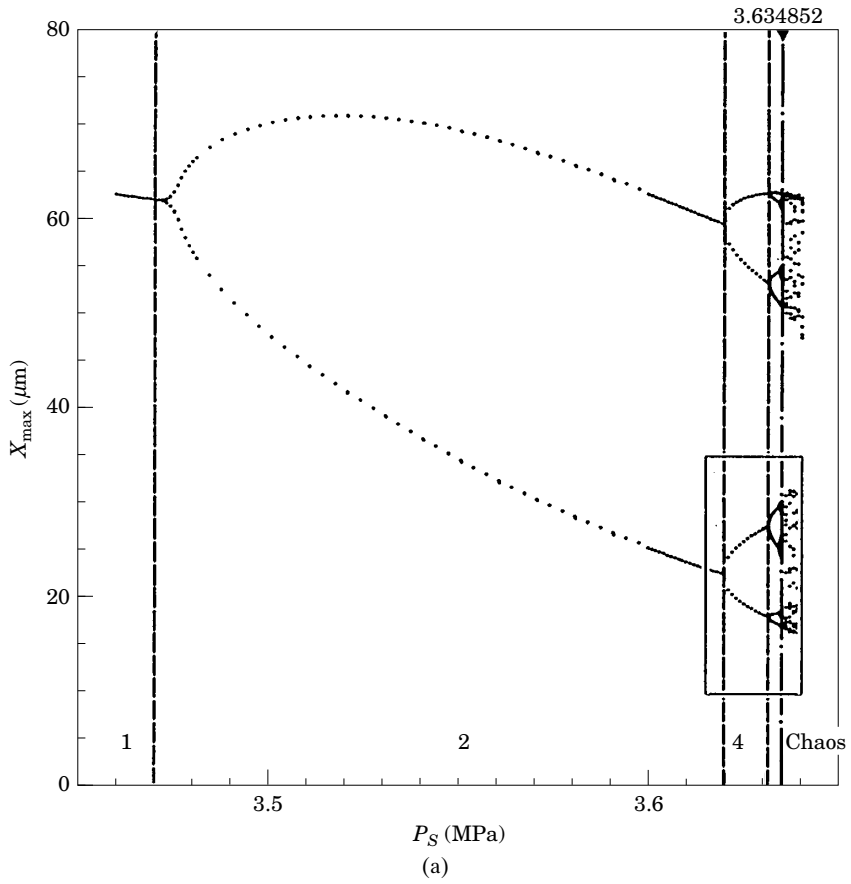

Figure 8. Enlargement of bifurcation map for period-doubling vibrations. (a) Bifurcation of $1 \rightarrow 2 \rightarrow 4 \rightarrow 8$; (b) bifurcation of $2 \rightarrow 4 \rightarrow 8 \rightarrow 16$; (c) bifurcation of $8 \rightarrow 16 \rightarrow 32 \rightarrow 64$.

solution, and let the state variable just after the nth collision at a certain time and the $(n+1)$th collision be

$$Y_n = (0, \dot{X}_n^+, P_{Cn}, Q_{On})^{\mathrm{T}}, \tag{21}$$

and

$$Y_{n+1} = (0, \dot{X}_{n+1}^+, P_{Cn+1}, Q_{On+1})^{\mathrm{T}}, \tag{22}$$

respectively, where $\dot{X}_n^+$, and $\dot{X}_{n+1}^+$ are the valve velocities just after the nth and $(n+1)$th collisions.

Setting the time interval between successive nth and $(n+1)$th collisions as Δt_n, Y_{n+1} is calculated by the following integral for the initial condition Y_n:

$$Y_{n+1} = \int_0^{\Delta t_n} F(Y, Y_n)\, \mathrm{d}t. \tag{23}$$

We consider the relation as a mapping from Y_n to Y_{n+1} which are discretized by successive collisions and represent the relation by

$$Y_{n+1} = f(Y_n). \tag{24}$$

By slightly shifting the initial condition from Y_n to $Y_n + \delta Y_n$, where δY_n is a small

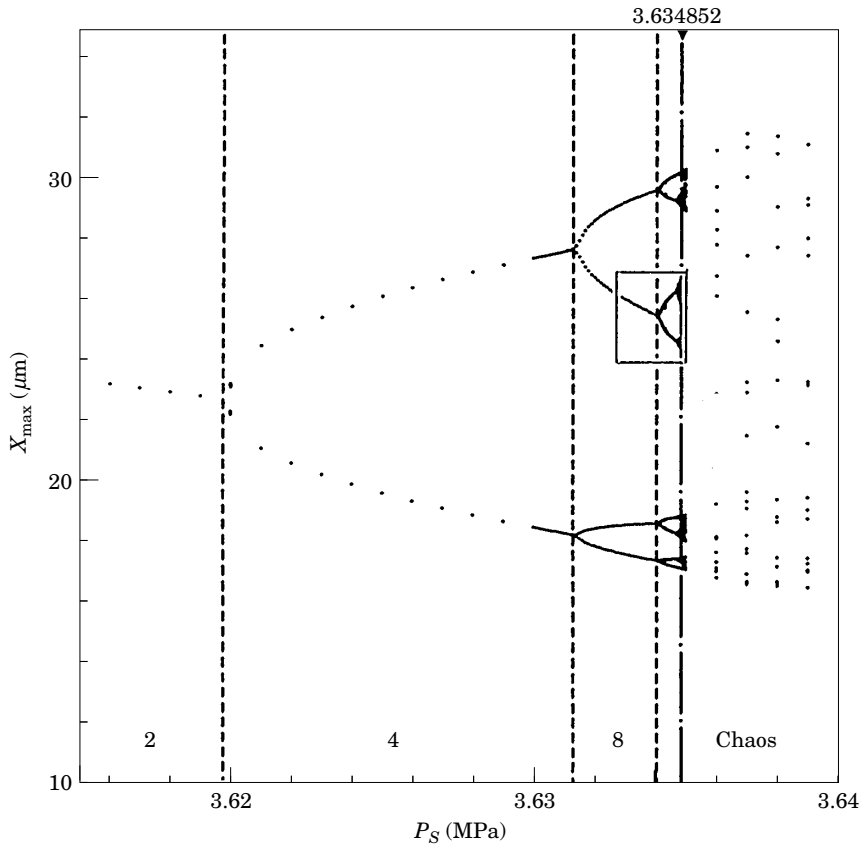

(b)

Figure 8. (*Continued.*)

perturbation whose direction coincides with Y_n, the state variable just after the successive collisions is given by

$$Y_{n+1} + \delta Y_{n+1} = \int_0^{\Delta t_n'} F(Y,\, Y_n + \delta Y_n)\, \mathrm{d}t, \tag{25}$$

where $\Delta t_n'$ means the time interval between the successive collisions for the slightly shifted infinitial conditions. From the above discussion, the Lyapunov exponent λ for the discrete dynamical system (24) can be approximated by

$$\begin{aligned} \lambda &= \lim_{N\to\infty} \frac{1}{N} \sum_{n=1}^{N-1} \log |f'(Y_n)| \\ &\simeq \frac{1}{N} \sum_{n=1}^{N-1} \log \frac{|\delta Y_{n+1}|}{|\delta Y_n|}. \end{aligned} \tag{26}$$

In order to examine the influence of the magnitude of small perturbations $|\delta Y_n|$ given as initial disturbances and of the iteration cycle N (the number of collisions) on convergence of the calculation for the Lyapunov exponent λ, the test calculations were carried out for $|\delta Y_n| = 10^{-8}$, 10^{-12}, 10^{-13} and the iteration cycle $N = 1500$. The operating condition of the system is chosen as $P_{Si} = 4{\cdot}0$ MPa and $P_S = 3{\cdot}7$ MPa. The results are shown in Figure 9.

As seen in Figure 9, two curves plotted by a solid line and a dotted line with open

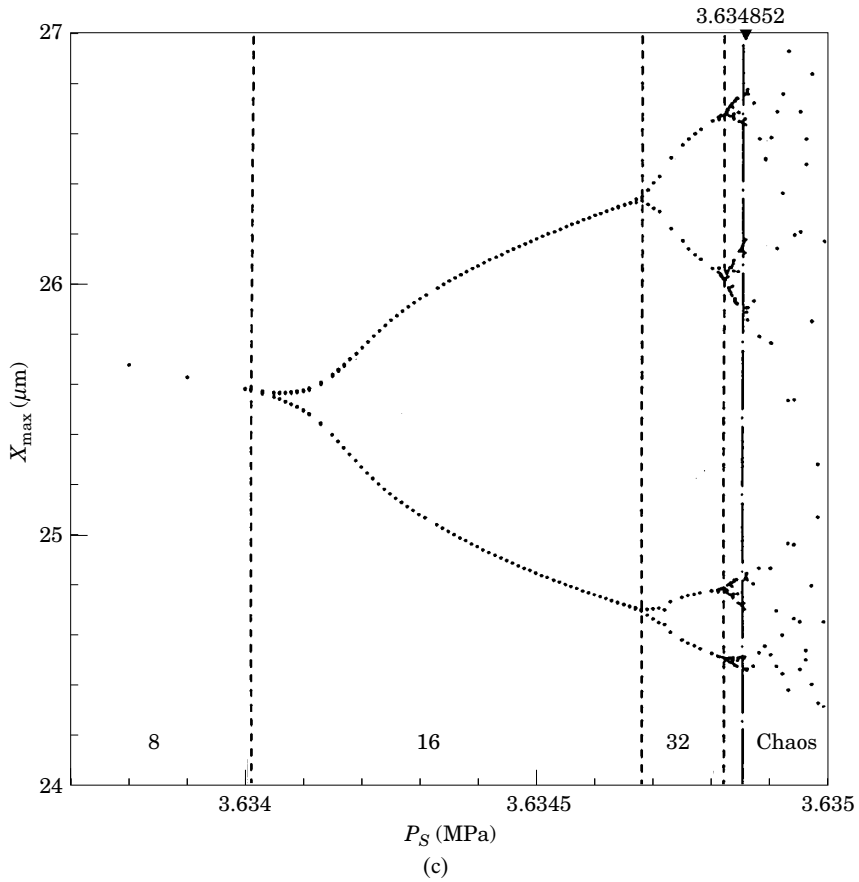

(c)

Figure 8. (*Continued.*)

circles (○) corresponding to $|\delta Y_n| = 10^{-12}$ and 10^{-8} converge to nearly the same value, and they do not show large changes for $N > 500$. On the other hand, the curve with closed circles (●) for the smallest perturbation $|\delta Y_n| = 10^{-13}$ converges to a slightly different value from the other curves, and the variation for $N > 500$ is somewhat larger than the others. This is considered to be caused by round-off errors; thus the calculation of λ was carried by using $|\delta Y_n| = 10^{-12}$.

Figure 10 shows the variation of λ with P_S. The positive region of λ coincides with the chaotic region in Figure 7, where points are densely distributed. In the region for the

TABLE 2

Bifurcation sequences

n	$2^{n-1} \rightarrow 2^n$	μ_n	$\mu_n - \mu_{n-1}$	Δ_n
1	1→2	3·47000	—	—
2	2→4	3·61974	0·14972	—
3	4→8	3·631291	0·01155	12·963
4	8→16	3·634090	0·00280	4·125
5	16→32	3·634689	0·000599	4·674
6	32→64	3·634820	0·000131	4·573

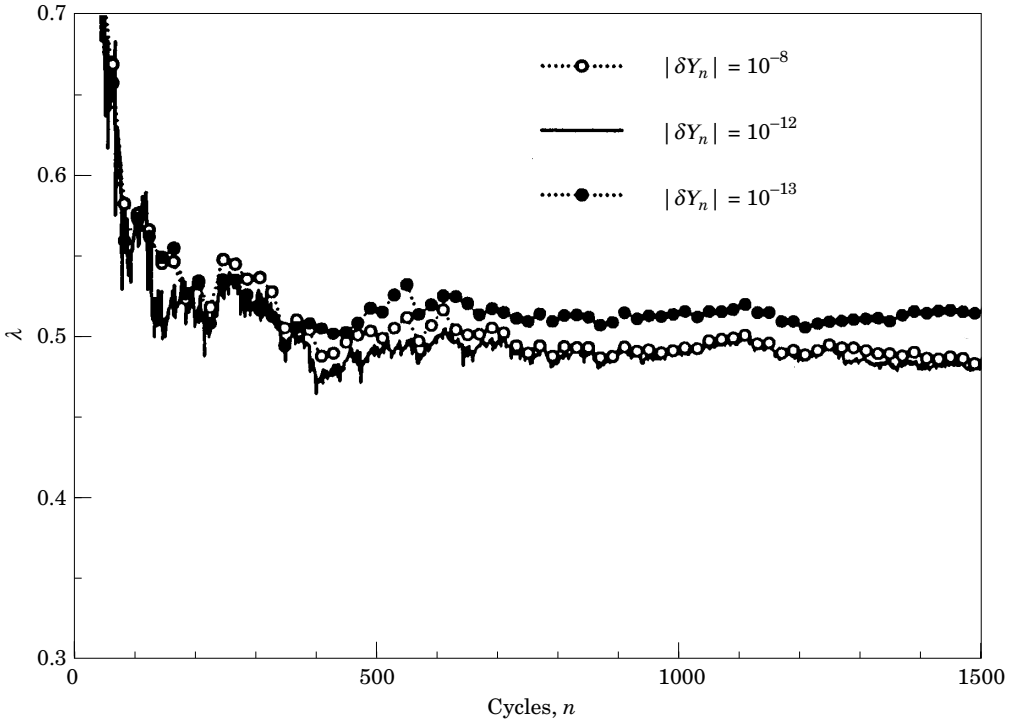

Figure 9. Convergence of Lyapunov exponent with cycle number n. (○) $\delta Y_n = 10^{-8}$; (—) $\delta Y_n = 10^{-12}$; (●) $\delta Y_n = 10^{-13}$.

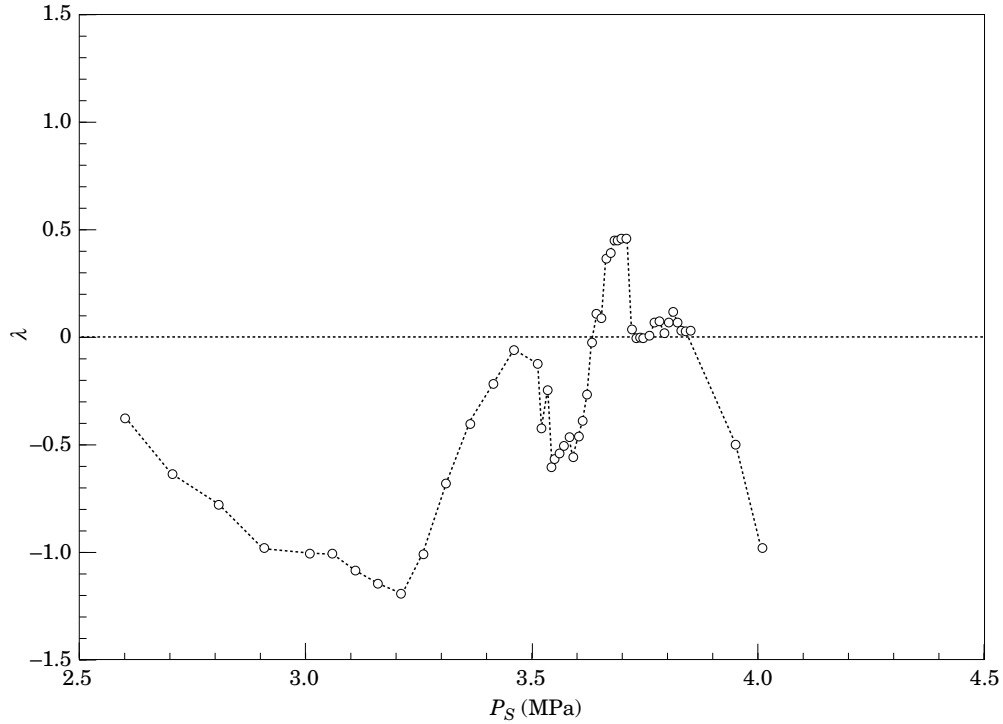

Figure 10. Lyapunov exponent with supply pressure ($P_{Si} = 4{\cdot}0$ MPa).

window of period-3 vibration, λ does not become negative, but it becomes nearly zero in this calculation.

5. CONCLUSIONS

We have numerically studied chaotic vibratory phenomena in a poppet valve circuit with a relatively short supply line by means of power spectra, a bifurcation diagram and Lyapunov exponents. It is clarified that the predominant dynamics are a period-doubling sequence culminating in chaos, followed by a reversal to period-1 motion at high values of the supply pressure, which is the system parameter varied. The period-doubling route to chaos is quantitatively confirmed by computation of the associated universal Feigenbaum number. Calculations of the largest positive Lyapunov exponent confirms the existence of chaos. This dynamical behaviour occurs for supply pressures lower than the cracking pressure of the poppet valve.

ACKNOWLEDGMENT

Support of this research was provided by Grant-in-Aid for Scientific Research of the Ministry of Education, Science and Culture.

References

Backé, W. & Rünnenburger, M. 1964 Zur Klärung des Verhaltens von Überdruckventilen. *Industrie Anzeiger* **86-98,** 2107–2116.

Feigenbaum, M. J. 1979 The universal metric properties of nonlinear transformations. *Journal of Statistical Physics* **21,** 669–706.

Funk, J. E. 1964 Poppet valve stability. *ASME Journal of Basic Engineering* **86,** 207–212.

Hayashi, S. & Mochizuki, T. 1987 Irregular vibrations occurring in a poppet valve circuit. In *Proceedings of* 2*nd Fluid Control Symposium,* pp. 115–120 (in Japanese).

Hayashi, S. & Ohi, K. 1988 Digital simulation of dynamic behaviors of poppet valve circuit. In *Proceedings 2nd International Symposium on Fluid Control, Measurement, Mechanics and Flow Visualization,* Sheffield, U.K., pp. 31–35.

Hayashi, S. & Mochizuki, T. 1989 Chaotic vibrations occurring in a hydraulic circuit (digital simulation and experimental study). In *Proceedings of 1st JHPS International Symposium on Fluid Power,* Tokyo, Japan, Vol. C2-4, pp. 475–482.

Hayashi, S. & Ohi, K. 1993 Global stability of a poppet valve circuit. *Journal of Fluid Control* **21,** 48–63.

Hayashi, S., Iizuka, Y. & Hayase, T. 1994a Numerical treatment of discontinuity due to collision. *Hydraulics and Pneumatics* **25,** 439–445 (in Japanese).

Hayashi, S., Hayase, T. & Kurahashi, T. 1994b Mechanism of hard self-excited vibration in poppet valve (the case of large valve lift). In *Proceedings* 4*th International Symposium on Fluid Control, Measurement and Flow Visualization,* Toulouse, France, Vol. 2, pp. 641–646.

Hayashi, S. 1995 Instability of poppet valve circuit. *JSME International Journal* C**38,** 357–366.

Kasai, K. 1968a On the stability of a poppet valve with an elastic support (1st report, considering the effect of the inlet piping system). *Transactions of Japan Society of Mechanical Engineers* **11–48,** 1068–1083.

Kasai, K. 1968b On the stability of a poppet valve with an elastic support (2nd report, considering the effect of the outlet piping system). *Transactions of Japan Society of Mechanical Engineers* **12–53,** 1091–1098.

Takenaka, T. & Urata, E. 1975 *Yurikigaku* (Dynamics of Hydraulics), pp. 48–50. Tokyo: Yoken-do (in Japanese).

Shaw, S. W. & Holmes, P. J. 1983 A periodically forced piecewise linear oscillator. *Journal of Sound and Vibration* **90,** 129–155.

Wolf, A., Swift, J. B., Swinney, H. L. & Vastano, J. A. 1985 Determining Lyapunov exponent from a time series. *Physica* **16**D, 285–317.

APPENDIX: NOMENCLATURE

A_L cross-sectional area of pipeline, $\pi d_L^2/4$
A_O opening area of orifice, $\pi d_O^2/4$
A_P cross-sectional area of valve seat, $\pi d_P^2/4$
a_P equivalent cross-sectional area of valve seat, $[\partial F/\partial P_C]_E$
C capacitance of valve chamber, V/β
C_O discharge coefficient of orifice
C_P discharge coefficient of poppet valve
C_{P0} discharge coefficient of poppet valve for large valve lift
c_P linearized discharge coefficient of poppet valve $[\partial Q_C/\partial P_C]_E$
c_X linearized flow gain of poppet valve, $[\partial Q_C/\partial X]_E$
d_L inner diameter of pipeline
d_O diameter of orifice aperture
d_P diameter of poppet valve seat aperture
e restitution coefficient of poppet to valve seat
F axial flow force acting on poppet
f_0 initial compression force of suspension spring, kX_i
h time stepsize in Runge–Kutta computation
I inertance of pipeline, $\rho L/A_L$
k spring constant of suspension spring
k_X hydraulic spring force, $[\partial F/\partial X]_E$
L supply pipeline length
m poppet mass
P_C pressure in valve chamber
P_{CE} static valve chamber pressure
P_O upstream pressure of orifice
P_S supply pressure
P_{Si} cracking pressure, f_0/A_P
p_C variational valve chamber pressure
Q_{OE} static flow
Q_O flow rate through orifice
Q_C flow rate through poppet valve
q_O variational flow rate through orifice
V volume of poppet chamber
X poppet valve displacement (valve lift)
X_E static valve lift
X_i initially compressed length of suspension spring
X_{ref} reference quantity for valve lift
x variational displacement of poppet valve
Δ Feigenbaum number
α half angle of poppet
β bulk modulus of working fluid (oil)
γ poppet valve factor
δ viscous damping coefficient
λ Lyapunov exponent
μ_n bifurcation point
ρ density of working fluid